Colloids and Surfaces B: Biointerfaces 267 (2026) 115909

Contents lists available at ScienceDirect

Colloids and Surfaces B: Biointerfaces

journal homepage: www.elsevier.com/locate/colsurfb

Development of a gene-activated scaffold using niosomes and minicircle DNA as a novel non-viral delivery platform to enhance cartilage repair

Junquera López-Seijas [a], Alba Iglesias-Fente [a], Claudio Intini [b,e], Marko Dobricic [b,c,d], Fergal J. O'Brien [b,c,d], Ana Rey-Rico [a,*]

[a] Gene & Cell therapy (G-CEL) Research Group, CICA - Centro Interdisciplinar de Química e Bioloxía, Departamento de Biología, Facultad de Ciencias, Universidade da Coruña, A Coruña, Spain
[b] Tissue Engineering Research Group (TERG), Department of Anatomy and Regenerative Medicine, Royal College of Surgeons in Ireland (RCSI), Dublin, Ireland
[c] Trinity Centre for Biomedical Engineering (TCBE), Trinity College Dublin, Dublin, Ireland
[d] Advanced Materials and Bio Engineering Research (AMBER) Centre, Dublin, Ireland
[e] Department of Biomedical Sciences, University of Cagliari, Monserrato, Italy

ARTICLE INFO

Keywords:
Gene-activated scaffold
Niosome
Minicircle DNA
SOX9
Chondrogenesis
MSCs

ABSTRACT

Gene therapy combined with advanced biomaterial-based delivery systems represents a powerful strategy to enhance chondrogenic differentiation of mesenchymal stem cells (MSCs), enabling the development of next-generation regenerative therapies for cartilage repair. In this context, gene-activated biomaterials provide a versatile tool for spatially and temporally regulating cell fate within three-dimensional (3D) microenvironments. Here, we combine collagen type I/type II-hyaluronic acid (CI/CII-HyA) scaffold with a novel non-viral gene delivery platform based on niosomes (DP20CQ) to deliver the master chondrogenic transcription factor SOX9 using either parental (PP) or minicircle (MC) plasmids, thereby promoting chondrogenesis in MSCs. After 28 days under chondrogenic conditions, DP20CQ-based scaffolds promoted a more favourable chondrogenic-to-hypertrophic profile than gene-free or Lipofectamine (LPF)-based scaffolds while preserving metabolic activity. Sustained SOX9 overexpression was evidenced in both PP and MC niosome-based systems at the gene and protein levels. Similarly, both systems showed an upregulation of key chondrogenic markers, including aggrecan (ACAN) and collagen type II (COLII), together with the concomitant downregulation of fibrocartilage (collagen type I, COLI) and hypertrophic (collagen type X, COLX) markers, with DP20CQ/MC exhibiting the highest expression ratios. Taken together, these findings demonstrate that DP20CQ-activated biomaterials enable efficient and sustained genetic regulation in MSCs within a 3D microenvironment, promoting the formation of hyaline-like cartilage while suppressing hypertrophic differentiation. This strategy constitutes a versatile gene-activated biomaterial platform with promising potential for cartilage regeneration.

1. Introduction

Articular cartilage injuries represent a persistent challenge in regenerative medicine due to the intrinsic avascular and aneural nature of the tissue, which severely limits its capacity for repair. While various surgical and biological alternatives exist, a major hurdle remains the inability to restore a stable hyaline cartilage matrix, frequently resulting in fibrocartilage formation that lacks the mechanical properties and biochemical profile necessary to support long-term joint function [1,2]. Consequently, the development of tissue-engineered strategies capable of recreating a physiologically relevant microenvironment and directing cellular fate toward a stable chondrogenic phenotype remains a critical research priority [3].

Mesenchymal stem cells (MSCs) have emerged as a promising cell population for cartilage tissue engineering due to their multipotency, accessibility, and capacity for chondrogenic differentiation under appropriate stimulation [1,4]. However, conventional chondrogenic induction methods, such as soluble growth factor delivery, often result in transient, non-localised responses and limited penetration within 3D matrices, leading to phenotypic instability owing to their short half-life [5,6]. These limitations compromise the ability of MSCs to sustain a stable chondrogenic phenotype, frequently resulting in incomplete

* Corresponding author.
E-mail address: ana.rey.rico@udc.es (A. Rey-Rico).

https://doi.org/10.1016/j.colsurfb.2026.115909
Received 7 April 2026; Received in revised form 9 June 2026; Accepted 9 June 2026
Available online 11 June 2026

extracellular matrix (ECM) maturation or hypertrophic differentiation.

Gene therapy offers a powerful alternative to traditional growth factor delivery, enabling the localised, sustained, and effective administration of pro-chondrogenic inputs [7]. Within this framework, several molecular regulators of MSC chondrogenesis have been investigated, including members of the transforming growth factor-β (TGF-β) superfamily, bone morphogenetic proteins (BMPs), and SOX transcription factors. However, many of these approaches remain limited by transient signalling or the induction of hypertrophic differentiation [8]. In this context, SRY-box transcription factor 9 (SOX9) has emerged as a central therapeutic target, acting as a master regulator of chondrogenesis, maintaining the hyaline cartilage phenotype through the upregulation of essential ECM genes, such as aggrecan (ACAN) and collagen type II (COLII), while repressing hypertrophic pathways [9–11]. The continuous expression of this lineage-defining factor is crucial for achieving stable cartilage repair [12].

Conventional vehicles for gene transfer to MSCs include viral and non-viral vectors. Despite their lower efficiency compared to viral vectors, non-viral systems, particularly cationic lipid-based nanocarriers, are increasingly preferred for clinical translation due to their superior safety profile, lower immunogenicity, and tunable physicochemical properties [11,13,14]. Liposomes are lipid nanocarriers that rely on electrostatic interactions between positively charged headgroups and the anionic phosphate backbone of nucleic acids, forming protective complexes that facilitate cellular uptake [15,16]. However, conventional liposome formulations are often associated with limited stability and dose-dependent cytotoxicity.

To overcome these limitations, niosomes have emerged as alternative vesicular systems in which phospholipids are replaced by non-ionic surfactants, conferring enhanced physicochemical stability, reduced toxicity, and lower production costs while preserving efficient nucleic acid complexation and delivery capabilities [17]. Among these, niosomes based on DOTMA as cationic lipid, polysorbate 20 or 80 as non-ionic surfactants, and chloroquine and cholesterol as helper lipid (DP20CQ and DP80CH, respectively) have demonstrated proper physicochemical characteristics and efficient transfection performance in human MSCs [18]. Particularly, DP20CQ niosomes have demonstrated their effectiveness in promoting chondrogenesis through the transfection of human MSC aggregate cultures [19].

Beyond the delivery vector, the architecture of the plasmid DNA critically influences transfection efficiency and expression longevity. Parental plasmids (PP), while widely used, contain bacterial backbone elements that increase plasmid size, reduce transfection efficiency, and may trigger epigenetic silencing or immune responses [20]. In contrast, minicircle plasmids (MC) eliminate the bacterial sequences, thereby offering a smaller genetic payload that enhances transfection efficiency, promotes more sustained transgene expression, and reduces inflammatory activation [21–23]. These characteristics are particularly relevant for SOX9, where continuous expression is necessary to drive and maintain stable MSC chondrogenesis.

However, the therapeutic potential of gene delivery approaches is often limited when vectors are administered in the absence of a supportive biomaterial environment, owing to poor spatial control and transient transgene expression. Gene-activated scaffolds constitute a versatile platform by integrating biomaterial structure with localised, nonviral gene delivery, enabling spatially controlled and temporally sustained regulation of MSC fate [3,8]. Importantly, these systems also function as instructive templates that support host cell infiltration, proliferation, and differentiation, enhancing endogenous cartilage repair processes.

This approach, integrating an engineered scaffold for therapeutic gene delivery and MSCs, has demonstrated positive outcomes in treating focal articular cartilage defects *in vitro* and *in vivo* [24,25].

In this context, scaffolds fabricated from a blend of collagen type-I (CI) and type-II (CII) with hyaluronic acid (HyA; CI/CII–HyA), in which HyA is physically entrapped within the collagen fibrillar network, provide a biomimetic microenvironment that supports chondrogenic differentiation, extracellular matrix deposition, and cell–matrix interactions resembling native cartilage tissue [26–28].

Mechanistically, collagen forms a structural framework that supports cellular adhesion and mechanical stability, whereas HyA contributes to hydration, viscoelasticity, and signalling interactions that favour chondrogenic maturation. In addition, CII actively promotes MSC chondrogenic maturation through interactions with specific protein domains, primarily mediated by integrin α2β1 engagement and downstream SMAD1 signalling [29].

In this study, we developed gene-activated CI/CII–HyA scaffolds incorporating an MSC population and DP20CQ niosomes complexed with either PP (DP20CQ/PP) or MC (DP20CQ/MC) encoding SOX9. Importantly, we compared for the first time the performance of PP and MC constructs delivered through a non-viral system within a collagen-based scaffold environment.

We evaluated how plasmid architecture and delivery vectors influence transfection efficiency in MSC two-dimensional (2D) monolayer culture, and downstream chondrogenic outcomes within a biomimetic 3D microenvironment. In addition, niosome-based gene-activated scaffolds were directly compared with LPF-based scaffolds, in which LPF was also complexed with both plasmid architectures, to assess the impact of vector selection on matrix deposition and hypertrophic progression.

Our findings demonstrate that, irrespective of the plasmid type used, SOX9 delivery via DP20CQ niosomes improves the chondrogenic profile of MSCs within CI/CII–HyA scaffolds and reduces hypertrophy, supporting the potential of refined non-viral gene-activated systems in guiding MSCs toward a more hyaline-like and phenotypically stable cartilage matrix. By combining a direct comparison of plasmid topologies with an MSC-optimised non-viral vector within a previously characterised 3D collagen-based matrix, this study provides comparative evidence to inform the rational design of gene-activated matrices for cartilage regeneration.

2. Materials and methods

2.1. Materials

Polysorbate 20 (P20, MW 1105 g/mol), polysorbate 80 (P80, MW 1064 g/mol), chloroquine (CQ, MW 515.5 g/mol), and papain (Carica papaya Latex) were obtained from Alfa Aesar (USA). 1,2-di-O-octadecenyl−3-trimethylammonium propane (D, DOTMA, MW 670.6 g/mol) was purchased from Angene (China). Dulbecco's Modified Eagle's Medium (DMEM), Phosphate-Buffered Saline (PBS), Fetal Bovine Serum (FBS), Penicillin/Streptomycin (P/S), GlutaMAX™, MEM Non-essential amino acids (MEM NEAA), OptiMEM™ reduced serum medium, Insulin-Transferrin-Selenium-A (ITS), dichloromethane, Insulin-Transferrin-Selenium-A (ITS) and cholesterol **95%** (CH, MW 386.7 g/mol) were sourced from Gibco -Thermo Fisher Scientific (USA). *SalI* and *XbaI* restriction enzymes, LB Agar, Halt™ protease, and phosphatase inhibitor cocktail (100X), AlamarBlue™ and BCA™ Protein Assay Kit were obtained from Thermo Fisher Scientific (USA). Lipofectamine™ Stem Reagent (LPF), Luria Broth (LB), SYBR™ Gold (10000 X), 5X annexin-binding buffer, Quant-iT PicoGreen dsDNA, and HiPure Plasmid Maxiprep Kit were purchased from Invitrogen - Thermo Fisher Scientific (USA). The Human SOX9 (Transcription factor SOX−9) ELISA Kit was acquired from FineTest (China). Recombinant TGF-β3 was obtained from Peprotech (USA).

The bovine Achilles tendon type I collagen was purchased from Collagen Matrix (USA), the porcine knee cartilage type II collagen from Symatese (France), and hyaluronic acid sodium salt derived from *Streptococcus equi* (1500–18000 kDa) from Contipro (Czech Republic). QIAzol Lysis Reagent was obtained from Qiagen (UK).

MN511A-SOX9 construct, kanamycin, growth media, and induction media were acquired from System Biosciences (USA). Annexin V APC

(1:10), Propidium Iodide staining solution (50 μg/mL; 1:100).

1,9-Dimethyl-Methylene Blue Dye (DMMB), sodium L-ascorbate, dexamethasone, acetic acid, L-proline, and sodium pyruvate were purchased from Sigma-Aldrich (USA). Chondroitin Sulfate C Sodium Salt was obtained from Toronto Research Chemical (Canada).

The First Strand cDNA Synthesis Kit for RT-PCR was obtained from Roche (Switzerland), RNeasy Protect Mini Kit from Qiagen (Germany), and PowerUp™ SYBR™ Green Master Mix from Applied Biosystems (USA).

The Laemmli sample buffer (#1610737), 2-mercaptoethanol (#1610710), Mini-PROTEAN TGX electrophoresis gels 4–20% (#4561094), Trans-Blot Turbo Mini 0.2 μm PVDF Transfer Packs (#1704156), 10x Tris/Glycine/SDS Buffer (#1610732), Clarity™ Western ECL Substrate (#1705060) were obtained from BioRad (UK).

The anti-SOX9 (ab182579) primary antibody and the goat anti-rabbit IgG H&L (HRP; ab6721) were purchased from Abcam (UK). GAPDH (sc−32233), anti-type I collagen (COLI; sc−293182), and mouse IgG Fc binding protein (m-IgG Fc BP; sc−525409) were obtained from Santa Cruz Biotechnology (USA). The anti-type II collagen (II-II6B3, COLII) antibody was purchased from DSHB (USA), and the anti-type X collagen (COLX) from Sigma Aldrich (USA). The biotinylated goat anti-mouse (IgG, H+L), the avidin–biotin complex (ABC)- horseradish peroxidase (HRP) kit, and Diaminobenzidine (DAB) Substrate Kit reagents were acquired from Vector Laboratories (USA).

2.2. Parental and minicircle DNA plasmid isolation and purification

The MN511A-SOX9 plasmid was generated by inserting the human SOX9 coding sequence into the MN511A−1 backbone (pMC.CMV-MCS-EF1α-GFP-SV40polyA), yielding the parental GFP/SOX9 plasmid (PP; 8587 bp). This parental construction served as the template for producing the corresponding minicircle GFP/SOX9 (MC; 4574 bp) [19].

Minicircle production was performed by transforming the *E. coli* ZYCY10P3S2T minicircle producer strain with the PP. Briefly, a single bacterial colony was inoculated into 2 mL of LB medium supplemented with 50 μg/mL kanamycin and cultured at 30 °C for 4–6 h under agitation (250 rpm). Subsequently, 1 mL of this starter culture was transferred into 200 mL of 1 × growth medium in a 1 L Erlenmeyer flask and incubated overnight at 37 °C with shaking at 250 rpm [30,31]. Once the exponential phase was reached (OD_{600} = 4–8, pH ≈ 7), 200–400 mL of 1 × induction medium was added, and the culture was further incubated for 4 h at 32 °C, followed by 1 h at 37 °C to induce the site-specific recombination process [19,30–32].

MC purification was performed using the HiPure Plasmid Maxiprep Kit according to the manufacturer's protocol, with appropriate modifications for minicircle recovery. Integrity and size were verified by restriction digestion (*SalI* and *XbaI*) and agarose gel electrophoresis [19].

In parallel, PP was propagated in *E. coli* STLB2 and purified using the same procedure.

2.3. Niosome production and nioplexes formation

Niosome formulations (DP20CQ and DP80CH) were formed by the thin-film hydration method using DOTMA as cationic lipid (2.5 mg; mole ratio = 1), polysorbate 20 (P20; 9.2 mg; mole ratio = 2) or polysorbate 80 (P80; 9.8 mg; mole ratio = 2) as non-ionic surfactants and chloroquine (CQ; 3.8 mg; mole ratio = 2) or cholesterol (CH; 2.9 mg; mole ratio = 2) as helper lipids, respectively [18,33]. In brief, all components were dissolved in dichloromethane and thoroughly mixed. Then, the organic solvent was evaporated under argon flow to form a dried film on the bottom of the glass flask, followed by the addition of 2.5 mL of OptiMEM™ (aqueous medium) to resuspend the film. The solution was sonicated for 40 s at 50 W using the UP200S Sonifier (Hielscher Ultrasound Technology, Germany).

Nioplexes were formed by mixing a fixed amount of PP or MC plasmids (300 ng per well for 2D monolayer experiments and 2 μg per scaffold for 3D scaffold experiments) and niosome solution to obtain 5/1 and 10/1 DOTMA/DNA mass ratios (w/w), corresponding to 2 and 5 nitrogenous (N) to phosphorous (P) ratios. Complexes were allowed to form for 30 min at room temperature before being added to cell monolayers or scaffolds and characterised as reported elsewhere [19].

2.4. Mesenchymal stem cells isolation and culture

Rat mesenchymal stem cells (MSCs, n = 2) were isolated from the bone marrow of early postnatal and juvenile Wistar rats, in accordance with Spanish law (32/2007), and with the previous approval of the Animal Ethical Committee of Galicia (accession number: 15/2127). Cells were cultured and expanded to passage 15 (early postnatal MSCs) or 7 (juvenile-derived MSCs) in high-glucose DMEM supplemented with 10% FBS, 100 U/mL P/S, 1% Glutamax, and 1% MEM NEAA. Cultures were maintained at 37 °C in a humidified atmosphere containing 5% CO_2 until further experimentation.

2.5. Transfection experiments in 2D monolayer cultures

For 2D transfection studies, early postnatal and juvenile-derived MSCs were seeded in 48- (GFP expression) or 24-well plates (SOX9 expression) at a density of 4×10^4 cells/cm^2 and allowed to attach for 24 h at 37 ºC. Then, cells were treated with nioplexes formed by complexing each niosome formulation, DP20CQ and DP80CH, with either PP or MC plasmid (0.32 μg/cm^2 of plasmid per well) at DOTMA/DNA ratios of 5/1 and 10/1.

Cells cultured in growth medium without nioplexes or cells transfected with the commercial reagent, LPF (1 μL/well; 0.32 μg/cm^2 of plasmid per well), were used as negative and positive controls, respectively. After incubation for 24 h at 37 ºC and 5% CO_2, cells were collected for analysis.

2.6. Evaluation of transfection efficiency and cell viability

GFP expression and cell viability were evaluated 24 h post-transfection using flow cytometry. Cells were washed with PBS, detached using trypsin, washed with several centrifugation steps, and resuspended in 5X annexin-binding buffer (diluted 1:5) containing Annexin V APC (1:1000), and Propidium Iodide staining solution (50 μg/mL; 1:100). Data acquisition and analysis were performed using CytExpert software using a CytoFLEX flow cytometer.

2.7. Determination of SOX9 expression in 2D transfection assays

SOX9 levels were assessed 24 h after transfection using ELISA. In brief, after washing the cells 3 times with PBS, lysates were prepared by adding a lysis buffer (50 mM Tris, 0.9% NaCl, 0.1% SDS, pH 7.3; 125 μL/well), supplemented with Halt™ protease and phosphatase inhibitor cocktail (1:100). Cells were then scraped to ensure complete recovery, and lysates were processed according to the manufacturer's protocol.

The concentration of SOX9 (ng/mL) in each sample was determined by measuring absorbance at 450 nm with a Synergy HTX plate reader (Biotek, USA) using a SOX9 standard calibration curve.

2.8. Biofabrication of highly porous biomimetic scaffolds

The collagen type I (CI) - collagen type II (CII) and hyaluronic acid (HyA) scaffolds (CI/CII-HyA) were fabricated using a freeze-drying method previously reported [26]. Collagen slurry was first prepared by blending bovine Achilles tendon type I collagen and porcine knee cartilage type II collagen (0.25%, w/v; 1:1 ratio) in 0.5 M acetic acid. Then, hyaluronic acid sodium salt (0.05% w/v; 1500–18000 kDa, *Streptococcus equi*) was dissolved in 0.5 M acetic acid and added dropwise to the collagen mixture [34]. This process results in a physically blended scaffold in which hyaluronic acid is entrapped within the

collagen matrix. The resulting CI/CII-HyA slurry was degassed, aliquots (0.3 mL) into stainless-steel molds (9.5 mm diameter and 4 mm height), freeze-dried for 48 h at –20 °C, and dehydrothermally crosslinked under vacuum (0.05 bar, 105 °C, 24 h; VacuCell oven, MMM, Germany) [34].

The structural and mechanical properties of these highly porous CI/CII–HyA scaffolds have been previously reported, supporting their suitability for cartilage tissue engineering [27,28,35].

2.9. Transfection studies in 3D gene-activated scaffolds

DP20CQ nioplexes with either PP or MC were prepared as described in *Niosome production and nioplexes formation* (Fig. 1). Nioplexes (15 μl; 1 μg DNA) were then loaded onto the scaffolds using a soak-loading approach, by adding them onto the upper surface of sterile CI/CII-HyA scaffolds and allowing them to adsorb for 15 min. Scaffolds were inverted, and the procedure was repeated on the opposite side, resulting in a total loading of 2 μg plasmid per gene-activated scaffold. As a positive control, gene-activated scaffold using LPF was prepared following the same procedure, with an equivalent amount of DNA.

Early postnatal MSC suspensions (25 μL of cell suspension; 2.5×10^5 cells) were seeded onto the top surface of each scaffold and incubated for 30 min to allow cell attachment. Scaffolds were then inverted, and the procedure was repeated on the opposite side, yielding 5×10^5 cells per scaffold. Cell-seeded CI/CII-HyA scaffolds without either DNA or the transfectant (gene-free scaffolds; C-) were prepared under identical conditions and served as negative controls. Constructions were cultured in growth medium (2 mL) for 24 h at 37 ºC.

After 24 h of incubation, gene-activated scaffolds were transferred to a new 24-well plate with chondrogenic differentiation medium serum-free high-glucose DMEM supplemented with 50 μg/mL ascorbic acid, 20 μg/mL proline, 100 nM dexamethasone, 1 × ITS, 0.11 mg/mL sodium pyruvate, and 20 ng/mL TGF-β3. Scaffolds were cultured at 37 ºC under static conditions for 7 or 28 days, with medium changes twice weekly, before being analysed in the different experiments.

To determine attachment efficiency, trypsin was added to the original well plate prior to scaffolds transfer to recover non-adherent cells. Cell suspensions were collected, centrifuged, and resuspended in growth medium. Cell number was determined using a haemocytometer, and attachment efficiency (%) was calculated as the ratio between the number of counted cells and the number of initially seeded cells × 100.

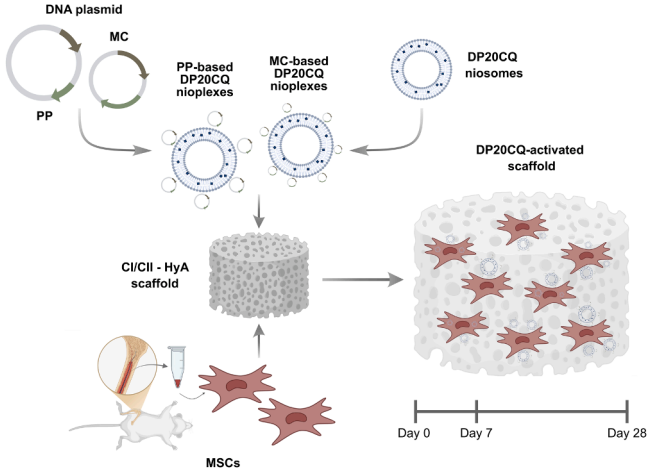

Fig. 1. Schematic representation of gene-activated scaffolds production. Niosomes based on polysorbate 20 and chloroquine (DP20CQ) complexed with parental (PP) or minicircle plasmid (MC) were put into contact with collagen type I/collagen type II, and hyaluronic acid (CI/CII-HyA) scaffolds before the incorporation of rat mesenchymal stem cells (MSCs) and incubation for 7 and 28 days.

2.10. DNA release profile

DP20CQ nioplexes or LPF lipoplexes with either PP or MC plasmids were loaded onto CI/CII-HyA scaffolds using the same procedure described before (*Transfection studies in 3D gene-activated scaffolds*). Gene-free and gene-loaded scaffolds were placed in the upper compartment of permeable supports (Transwell Permeable Supports, Life Technologies, Darmstadt, Germany; pore size 0.4 μm) located in 24-well plates containing PBS (500 μL in the lower compartment). Then, PBS (100 μL) was added to the upper compartment, and plates were incubated at 37 ºC under static conditions for 28 days.

At predetermined time intervals (0.25, 1, 3, 5, 7, 14, 21, and 28 days), aliquots from the lower compartment were collected, immediately frozen at –20 °C, and replaced with an equal volume of fresh PBS.

The amount of DNA released from CI/CII-HyA scaffolds in the collected aliquots was quantified by SYBR™ Gold nucleic acid stain, previously decomplexed of nioplexes with 7% SDS [10]. Fluorescence was measured in black 96-well plates using a Synergy HTX Plate Reader at excitation and emission wavelengths of 485 nm and 528 nm, respectively.

2.11. Scanning electron microscopy (SEM)

Gene-activated scaffolds were prepared using the same procedure described above (*Transfection studies in 3D gene-activated scaffolds*). Constructions were then fixed in 2% glutaraldehyde for 3 h at room temperature before being dehydrated through a graded ethanol series and dried using a critical point dryer.

Empty CI/CII-HyA scaffolds (C–) or gene-free CI/CII-HyA scaffolds containing only cells (C-) were processed in parallel.

The dried samples were sputter-coated with gold and examined using a JEOL JSM−6400 scanning electron microscope (JEOL USA Inc., Peabody, MA, USA) [10].

2.12. Analysis of gene expression regulating chondrogenesis

After 7 and 28 days of culture, gene-activated CI/CII-HyA scaffolds were lysed with QIAzol reagent, and total RNA was extracted using the RNeasy Protect Mini Kit according to the manufacturer's instructions. Reverse transcription was carried out using 250 ng of RNA with the First Strand cDNA Synthesis Kit for RT-PCR (AMV) to generate cDNA. Subsequently, 10 ng of cDNA was amplified by real-time PCR (qRT-PCR) using the PowerUp™ SYBR™ Green Master Mix on a QuantStudio 3 System (Applied Biosystems, USA).

The PCR conditions were set as follows: an initial denaturation from 50 ºC to 95 ºC at 1.6 ºC/s for 2 min, followed by 40 cycles of denaturation at 95 ºC for 15 s, annealing and extension at 60 ºC for 1 min each. A final melting curve analysis was conducted from 95 ºC to 65 ºC at 1.6 ºC/s and then to 95ºC at 0.5 ºC/s. Primers sequences are listed in Table 1, and all reactions were performed with a final primer concentration of 400 nM. Gene expression levels were normalised to GAPDH expression, and relative quantification was calculated using the $2^{-\Delta\Delta Ct}$ method [19,36].

2.13. Analysis of pro-chondrogenic SOX9 protein expression

Western blot analysis was performed on days 7 and 28 to assess SOX9 relative protein expression (both endogenous and transgene forms) in gene-activated CI/CII-HyA scaffolds [25]. Total protein was extracted, and aliquots (15 μg for day 7 and 10 μg for day 28) were denatured in Laemmli sample buffer containing 2-mercaptoethanol and separated by SDS-PAGE using Mini-PROTEAN TGX gels at 100 V for 1 h. Proteins were transferred onto 0.2 μm PVDF membranes using the Trans-Blot Turbo Transfer System.

Membranes were blocked with 5% (w/v) BSA in tris-buffered saline (TBS) with 0.1% Tween−20 (TBST) and incubated overnight at 4 °C with a primary rabbit anti-SOX9 (1:1000). After three washes with

Table 1
List of genes and primer sequences analysed by qRT-PCR. Primers were designed and used to analyse the expression levels of target genes.

Target gene	Forward sequence (5'−3')	Reverse sequence (5'−3')
Aggrecan (ACAN)	CCCAAACAGCAGAAACAGCC	CACTCATCAATGTCTGCAGCG
Type I collagen (COLI)	GGCCAAGAAGACATCCCTGA	CAGGTTTCCACGTCTCACCA
Type II collagen (COLII)	ATTGCCTACCTGGACGAAGC	TCAACAATGGGAAGGCGTGA
Type X collagen (COLX)	ATTGCCTACCTGGACGAAGC	TCAACAATGGGAAGGCGTGA
SRY (sex determining region Y)-box 9 (SOX9)	CCCCAACAGATCGCCTACAG	TCGTACTGTGAGCGGGTGAT
Green Fluorescent Protein (GFP)	GGCTACTACAGCTTCGTGGT	GGTGTTGCTGTGCAGCTCCT
Glyceraldehyde 3-phosphate dehydrogenase (GAPDH)	CCAGAGGGTGGCCTTGAAAT	GTGAAGCTCCCAATGTCCCA

TBST, membranes were incubated for 1 h at room temperature with HRP-conjugated goat anti-rabbit IgG (1:2000). Following additional washes, membranes were treated with enhanced chemiluminescence (ECL) substrate and imaged on a ChemiDoc MP Imaging System (Bio-Rad, UK). Membranes were stripped (0.2 M glycine, 0.1% SDS, 1% Tween−20, pH=2.2), re-blocked, and re-probed with anti-GAPDH (1:1000), followed by HRP-conjugated secondary antibody (1:2000).

Relative protein expression levels were quantified by densitometric analysis of band intensities using ImageJ software, normalised to the corresponding GAPDH signal for each sample.

2.14. Metabolic activity assay

AlamarBlue™ assay was performed as a non-destructive indicator of cellular metabolic activity at days 0, 3, 7, 14, 21, and 28 of culture [26,37]. Briefly, a 10% (v/v) AlamarBlue™ solution in culture medium was applied to each gene-activated CI/CII-HyA scaffold and incubated for 1 h at 37 °C. To assess metabolic activity, fluorescence was measured at excitation and emission wavelengths of 560 nm and 590 nm, respectively, using an Agilent Cary Eclipse Fluorescence Spectrophotometer (Agilent, USA). Metabolic activity per scaffold was calculated and normalised to cell-seeded CI/CII-HyA scaffolds at day 0.

2.15. Biochemical quantification of proteoglycans and DNA

Proteoglycans and DNA contents were quantified at 28 days following scaffold digestion. Gene-activated CI/CII-HyA constructs were washed with PBS and digested overnight at 65 °C in 0.01% papain solution. The proteoglycan content was determined using the dimethylmethylene blue (DMMB) assay, with chondroitin sulphate C as the standard [10,19]. Briefly, 250 μL of DMMB dye and 5 μL of D-cysteine hydrochloride monohydrate solution were added to 35 μL of each digested sample (or standard) in a 96-well plate. Absorbance at 525 nm was recorded using a Synergy HTX Plate Reader, and the proteoglycan concentration was calculated using a standard calibration curve [19].

DNA content was quantified using the Quant-iT™ PicoGreen® dsDNA assay according to the manufacturer's protocol. Fluorescence was measured at 485 nm excitation and 538 nm emission using a Synergy HTX Plate Reader [38].

2.16. Histological and immunohistochemical evaluation of extracellular matrix (ECM) deposition

After 28 days of culture, gene-activated CI/CII-HyA scaffolds were rinsed with PBS, fixed with 4% paraformaldehyde for 1 h at room temperature, dehydrated, and embedded in paraffin, following established protocols [25]. Paraffin sections (7 μm) were stained with 2% Alcian Blue (pH 2.5) to assess glycosaminoglycan-rich extracellular matrix deposition.

For immunohistochemistry, endogenous peroxidase activity was blocked, and sections were incubated with primary antibodies against collagen type I (1:100), collagen type II (1:10), and collagen type X (1:200). After washing, sections were incubated with a biotinylated secondary antibody and detected using the ABC-HRP detection system with DAB as the chromogen [11,19,36].

Sections were imaged using a Lionheart FX digital microscope (BioTek, USA). Histomorphometric analysis was performed using ImageJ. For each experimental group and replicate, three standardised regions of interest were quantified at 20 × magnification. Staining intensity was expressed as pixel intensity.

2.17. Statistical analysis

2D experiments were performed using MSCs from two independent rat donors (early postnatal and juvenile). Each experiment was repeated at least twice, with three technical replicates per condition. Gene-activated scaffolds assays were conducted using MSCs from a single early postnatal donor, with a minimum of two independent biological replicates and six technical replicates per condition.

Statistical analyses were performed using Prism GraphPad (GraphPad Software, USA). Data normality was assessed using the Shapiro–Wilk test and homogeneity of variances using Levene's test. Depending on data distribution and experimental design, one- or two-way ANOVA followed by Tukey's post-hoc test was applied for parametric data, whereas the Kruskal–Wallis test was used for non-parametric datasets. Statistical significance was defined as $p < 0.05$.

3. Results

3.1. Minicircle production

A 4.6 kb minicircle plasmid was generated from the parental 8.6 kb plasmid through arabinose-induced expression of the ΦC31 integrase system (Fig. 2). Upon recombination, the eukaryotic expression cassette was excised from the parental backbone, while the *I-SceI* endonuclease selectively degraded the remaining 4.0 kb bacterial sequence. Successful minicircle production and backbone removal were confirmed by agarose gel electrophoresis (data not shown).

3.2. In vitro 2D transfection of MSCs with niosome formulations

To identify the most efficient niosome formulation and DOTMA/DNA ratio for transfecting primary MSCs derived from early postnatal and juvenile rats (MSCs), DP20CQ and DP80CH niosomes were complexed with either PP or MC plasmids and applied to 2D MSC cultures. Transfection efficiency was assessed by GFP expression levels using flow cytometry.

A consistent trend in GFP expression was observed across both cell sources (Fig. 3**A** and **B**). DP20CQ nioplexes always achieved significantly higher GFP expression than DP80CH nioplexes, irrespective of the DOTMA/DNA ratio tested. These differences between both formulations were especially pronounced in the 10/1 DOTMA/DNA ratio, where DP20CQ demonstrated an evident superiority (up to 8.97- and 5.81-fold increase in early postnatal and juvenile, respectively; $p < 0.001$). Notably, DP20CQ complexed with PP or MC outperformed the positive control, LPF (up to 1.89- and 2.90-fold increase in early postnatal and juvenile, respectively; $p < 0.05$). In contrast, no significant differences in GFP levels were observed between PP and MC plasmids regardless of

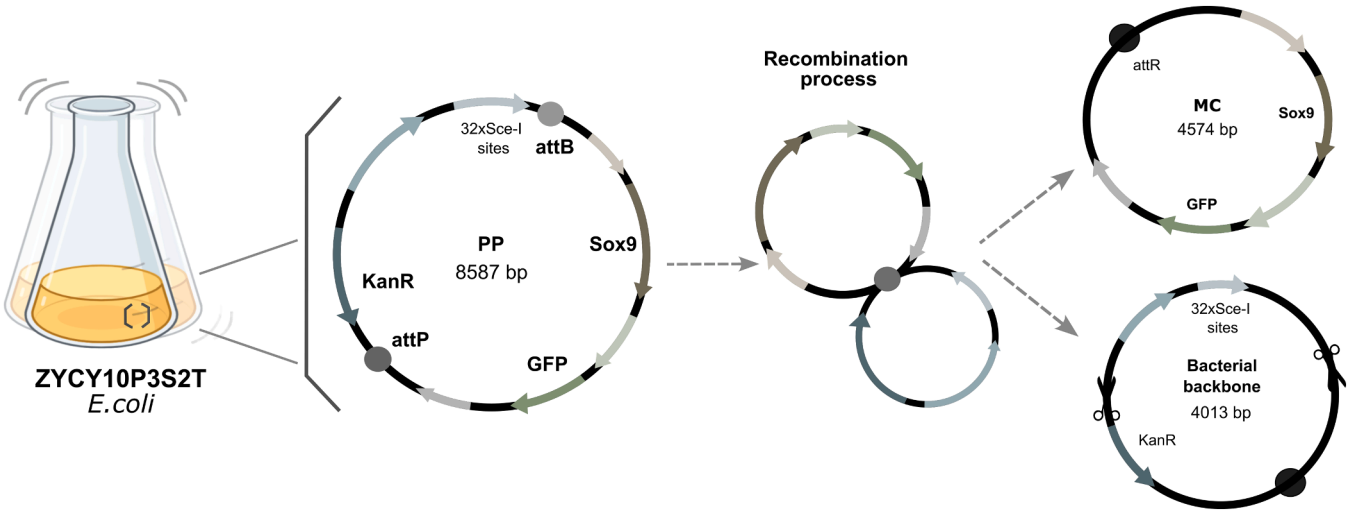

Fig. 2. Schematic production process and representation of PP and MC plasmids. DNA map composition of the parental plasmid (PP; MN511A-SOX9; pMC. CMV-MCS-EF1α-GFP-SV40poly A plasmid; 8587 bp), minicircle plasmid (MC; 4574 bp), and bacterial backbone (4013 bp).

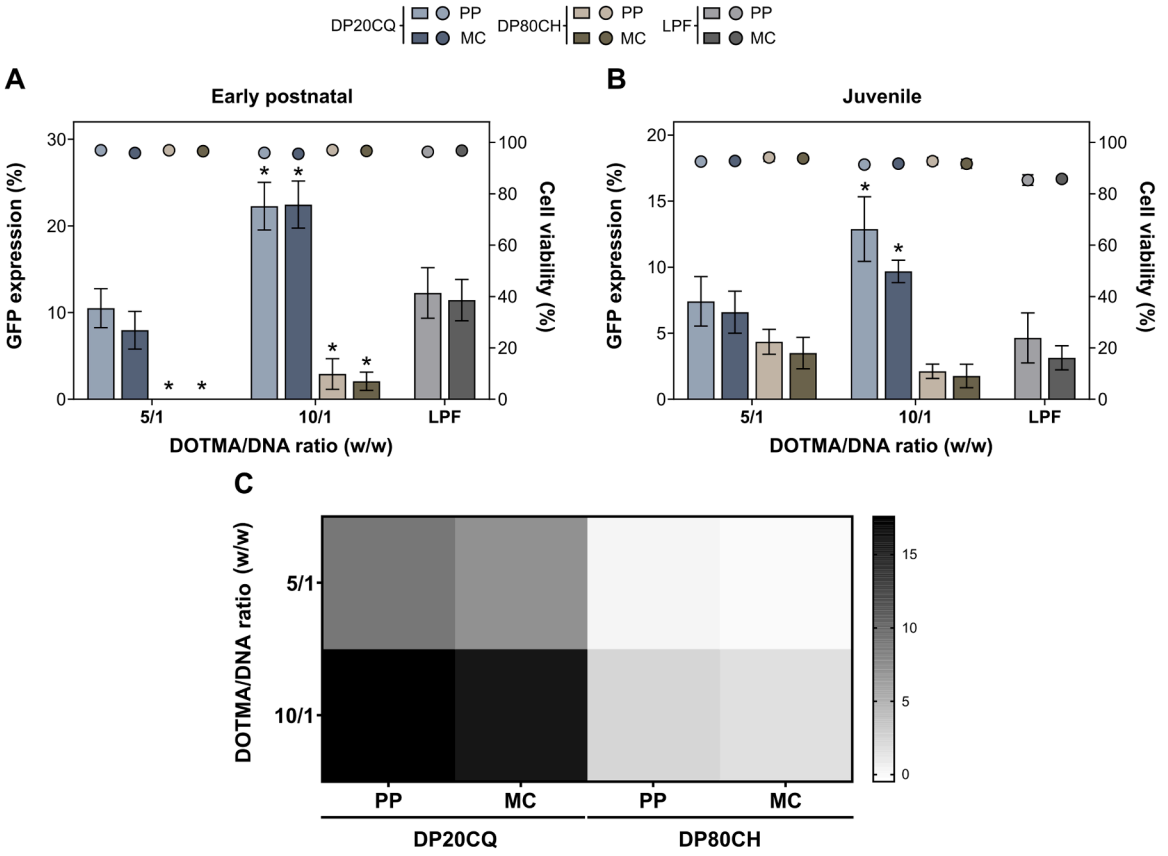

Fig. 3. Optimization and validation of DP20CQ and DP80CH niosomes in early postnatal and juvenile rMSC monolayers. GFP expression (%; bars; left y-axis) and cell viability (%; symbols; right y-axis) determined by flow cytometry after transfection of (**A**) early postnatal and (**B**) juvenile rMSC monolayers with niosomes based on polysorbate 20 and chloroquine (DP20CQ; blue) or polysorbate 80 and cholesterol (DP80CH; brown) complexed with parental plasmid (PP; light blue or light brown, respectively) or minicircle plasmid (MC; dark blue or dark brown, respectively). Data are shown as mean ± SD. * depicts $p < 0.05$, when comparing each formulation combined with a given plasmid type at different DOTMA/DNA ratios to LPF control group, n = 3. (**C**) Greyscale heatmap representing GFP expression levels (%) across two rMSC sources, where black denotes the highest and white the lowest transfection efficiency achieved.

the formulation used ($p > 0.172$).

Of note, cell viability was preserved across all conditions (> 91%), indicating that the niosome formulations maintained cytocompatibility in MSCs under 2D culture conditions. Conversely, a slight reduction in viability was observed in juvenile MSCs treated with LPF-based complexes, with values decreasing to approximately 85%.

To integrate the results obtained and enable direct comparison of transfection performance between the two niosome formulations in both MSC sources, a greyscale heatmap was generated (Fig. 3**C**). The squares corresponding to DP20CQ formulations displayed markedly darker

intensities compared to those of DP80CH, further confirming the superior efficiency of DP20CQ. Additionally, when comparing both DOTMA/DNA ratios within the same formulation, the 10/1 showed the highest intensities. No clear differences in intensity were observed between the two plasmids, suggesting similar performance under the tested conditions.

The concentration of SOX9 protein (ng/mL) were quantified by ELISA to confirm transgene expression following transfection (Figure S1). All formulations resulted in detectable SOX9 protein levels in MSCs from both sources compared with their respective untransfected controls. In early postnatal MSCs, both niosome- and LPF-based scaffolds achieved statistically significant increases ($p < 0.043$). In contrast, in juvenile MSCs, only LPF/MC-based scaffolds led to substantial differences ($p < 0.046$).

Based on these results, the DP20CQ formulation at a DOTMA/DNA ratio of 10/1 was selected for subsequent experiments in CI/CII-HyA scaffolds (Fig. 4**A**).

3.3. MSC attachment and metabolic activity in CI/CII-HyA gene-activated scaffolds

SEM imaging (Fig. 4**B**) was performed on empty scaffolds (C–), scaffolds seeded with MSCs without either the DNA or the transfectant (gene-free scaffolds; C-), and gene-activated scaffolds containing MSCs and either DP20CQ nioplexes or LPF lipoplexes.

Across all conditions, CI/CII-HyA scaffolds revealed an interconnected macroporous structure, with cells displaying a well-spread morphology and integration within the scaffold architecture. Moreover, successful incorporation of both DP20CQ and LPF complexes within the CI/CII-HyA scaffolds was clearly evidenced, regardless of the plasmid used.

Cell seeding efficiency was assessed after 24 h to evaluate the adherence capacity of MSCs to the different gene-activated scaffolds. As shown in Fig. 4**C**, comparable attachment yields were observed among the control group and all transfected conditions ($p > 0.05$).

Likewise, the metabolic activity of MSCs on CI/CII-HyA scaffolds was measured at different time points after seeding as a non-invasive indicator of cellular health (Fig. 4**D**). The delivery of DP20CQ and LPF complexed with PP or MC from the scaffolds did not compromise the metabolic activity of cells, which remained above control values throughout the culture period. Notably, PP- and MC-DP20CQ complexes were associated with a marked increase in metabolic activity on day 3 (up to 1.8-fold increase), after which values converged and remained similar across all groups for the 28 days.

Cumulative DNA release from CI/CII-HyA gene-loaded scaffolds was monitored for 28 days to characterise the release kinetics of DP20CQ- and LPF-based complexes (Fig. 4**E**). All gene-activated scaffolds exhibited an initial burst phase within the first days of incubation, followed by a slower release and subsequent plateau from day 14 onwards. DP20CQ-based scaffolds showed higher cumulative DNA release than their LPF counterparts, with DP20CQ/PP complexes consistently releasing more DNA than DP20CQ/MC. In contrast, LPF/PP scaffolds displayed a more moderate release profile than LPF/MC ($p < 0.05$).

3.4. MSCs chondrogenesis in CI/CII-HyA-gene activated scaffolds

Gene-free and gene-activated scaffolds were cultured for 7 or 28 days in chondrogenic medium before analysis. Samples collected at both time points were examined by qPCR and western blot, whereas histological, immunohistochemical, histomorphometric, and biochemical analyses were performed on samples cultured for 28 days.

qPCR was performed to compare the expression of total SOX9

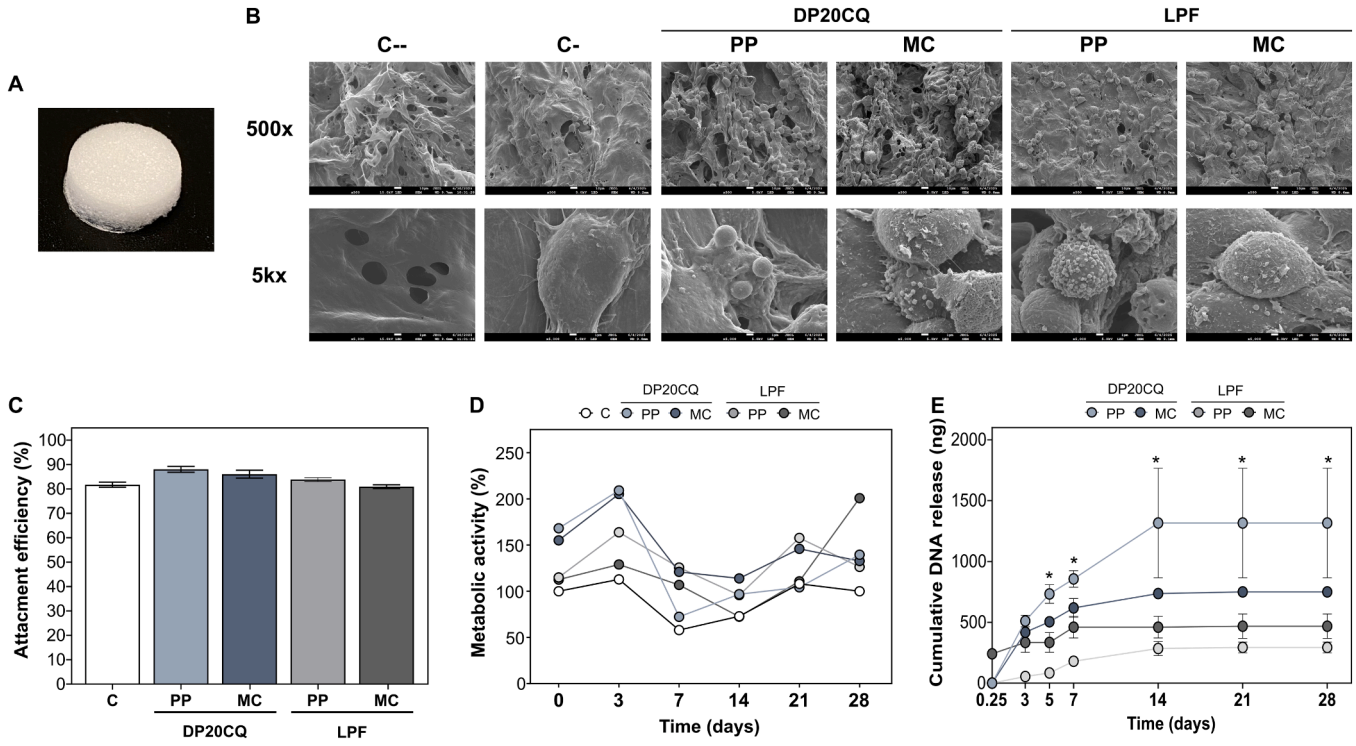

Fig. 4. SEM, cellular attachment, and metabolic activity of MSCs in CI/CII-HyA-gene activated scaffolds. (**A**) Illustrative macroscopic image of a CI/CII-HyA scaffold. (**B**) Representative SEM images (magnification: 500 × and 5000 ×) of empty CI/CII-HyA scaffolds (C–), CI/CII-HyA scaffolds containing only early postnatal MSCs (C-), and CI/CII-HyA seeded scaffolds after transfection with niosomes based on polysorbate 20 and chloroquine (DP20CQ) or Lipofectamine (LPF) complexed with either parental (PP) or minicircle (MC) plasmids. (**C**) Quantification (bars) of cell attachment efficiency 24 h post-seeding. (**D**) Cellular metabolic activity per scaffold (symbols and lines) was determined and normalized to the control group (white symbols, black line) at day 0 after 0, 3, 14, 21, and 28 days in culture. (**E**) Cumulative DNA release (symbols and lines) of DP20CQ and LPF complexed with either PP and MC loaded in CI/CII-HyA scaffolds after 0.25, 3, 5, 7, 14, 21, and 28 days.* depicts $p < 0.05$, when comparing DP20CQ formulation combined with a given plasmid type with the corresponding LPF control group at the same time point.

(transgene and endogenous), GFP transgene, chondrogenic markers (ACAN, COLII), and hypertrophic markers (COLI, COLX) in gene-activated scaffolds with nioplexes or lipoplexes, and gene-free scaffolds (Fig. 5 and Fig. 6).

After 7 days in culture, DP20CQ- and LPF-based scaffolds exhibited increased SOX9 and GFP mRNA expression relative to gene-free scaffolds (Fig. 5**A,** upper graphics). Notably, PP complexes displayed significant differences compared to the gene-free control ($p < 0.05$) in both transgenes, while MC, only when complexed with DP20CQ, achieved a marked upregulation of SOX9 expression ($p < 0.05$). At 28 days, both DP20CQ and LPF formulations complexed with either PP or MC were effective in enhancing SOX9 and GFP expression compared to the control (Fig. 5**A,** lower graphics), although statistical significance was observed only for DP20CQ complexed with PP ($p < 0.05$).

These findings were supported by western blot analysis, which confirmed the presence of SOX9 protein in gene-activated scaffolds after 7 (Fig. 5**B,** upper panel) and 28 days (Fig. 5**B**, lower panel). Densitometric analysis of bands at 28 days revealed modest increases in SOX9 protein levels, with DP20CQ complexed with PP and MC showing ~1.10- and 1.24-fold increase compared to gene-free control, respectively, compared to ~ 1.05- and 1.01-fold increase for LPF-based systems.

An analysis of downstream chondrogenic targets directly regulated by SOX9 at 7 days (Fig. 6**A,** left panels) revealed a slight upregulation of ACAN and COLII on DP20CQ-based scaffolds, without reaching statistical significance relative to the gene-free control ($p > 0.062$). In contrast, LPF-based scaffolds displayed a significant increase in these same markers compared to controls ($p < 0.011$).

After 28 days in culture (Fig. 6**A**, right panels), the ability of gene-activated scaffolds to promote MSC chondrogenic differentiation became more evident, showing an upregulation of ACAN and COLII in MSCs cultured on both types of gene-activated scaffolds relative to the gene-free control, although only LPF complexed with MC led to a significant enhancement ($p < 0.04$).

In parallel, fibrocartilage and hypertrophic marker expression revealed a clear dependence on the delivery system (Fig. 6**B**). LPF-based scaffolds significantly upregulated COLI expression at both 7 and 28 days ($p \leq 0.007$), particularly in MC-loaded scaffolds, whereas DP20CQ-based scaffolds did not induce COLI expression at any time point. A similar trend was observed for COLX, with LPF scaffolds significantly increasing its expression, especially under LPF/PP conditions ($p < 0.05$). In contrast, DP20CQ scaffolds reduced COLX expression relative to controls, although this reduction did not reach statistical significance ($p \geq 0.06$).

To further evaluate the balance between chondrogenic and hypertrophic responses, expression ratios associated with cartilage-like matrix synthesis and hypertrophic progression (ACAN/COLI, ACAN/COLX, COLII/COLI, COLII/COLX) were calculated (Fig. 6**C**).

At day 7, ACAN/COLI and COLII/COLI ratios (Fig. 6**C,** left panels) indicated an early shift toward a chondrogenic gene expression profile in MSCs cultured on gene-activated scaffolds. Notably, ACAN/COLX and COLII/COLX ratios (Fig. 6**C,** right panels) were significantly higher in DP20CQ-activated scaffolds compared to LPF-based systems and to gene-free controls ($p < 0.03$), suggesting enhanced chondrogenesis with reduced hypertrophic progression.

At 28 days, DP20CQ-based scaffolds maintained the highest ACAN/COLI and COLII/COLI ratios across all comparisons. However, statistical significance was only reached for the ACAN/COLI when DP20CQ/MC scaffolds ($p < 0.016$), while similar trends were observed for ACAN/COLX and COLII/COLX.

Proteoglycan deposition was quantified after 28 days to evaluate extracellular matrix formation (Fig. 7**A**). Both DP20CQ- and LPF-based scaffolds reached significantly higher proteoglycan content compared to gene-free scaffolds ($p < 0.019$), although no significant differences were observed between delivery systems or plasmid types.

An estimation of the DNA content per scaffold (Fig. 7**A**) revealed a significant increase across all transfected groups (666.24 ± 85.00 ng/scaffold) relative to the gene-free scaffolds (478.44 ± 14.83 ng/scaffold;

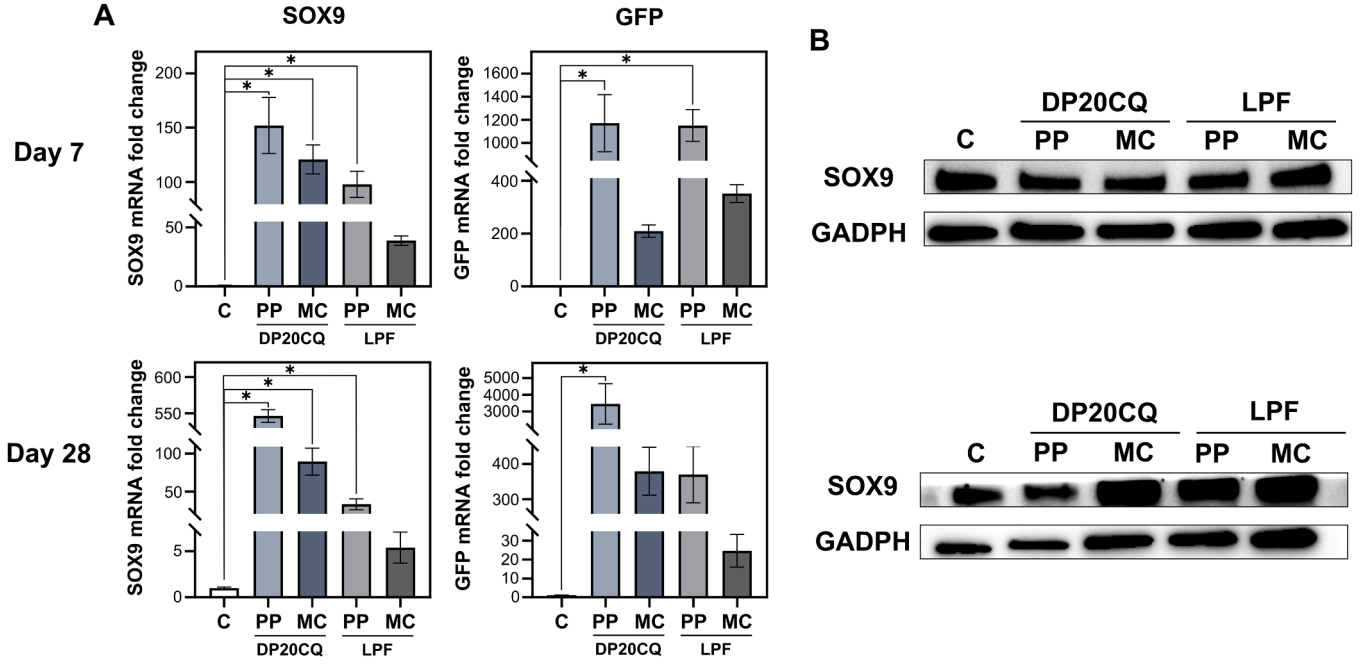

Fig. 5. qPCR analyses transfection in CI/CII-HyA gene-activated scaffolds. (**A**) Expression (bars) of SOX9 and GFP, as the transgenes present in parental (PP) and minicircle (MC) plasmids in gene-activated scaffolds cultured 7 (upper graphics) and 28 (lower graphics) days in chondrogenic medium (negative control; white) and transfected with niosomes based on polysorbate 20 and chloroquine (DP20CQ; blue) or Lipofectamine (LPF; grey) and complexed with either PP (light blue or light grey, respectively) or MC (dark blue or dark grey, respectively). Ct values were normalized to GADPH, and fold inductions were calculated considering the $2^{-\Delta\Delta Ct}$ method relative to the negative control. * depicts $p < 0.05$ when compared to the negative control, n = 3. (**B**) Representative western blot images showing SOX9 and GAPDH protein bands detected from the same membrane following stripping and reprobing in MSCs at days 7 (upper panel) and 28 (lower panel) under the indicated experimental conditions.

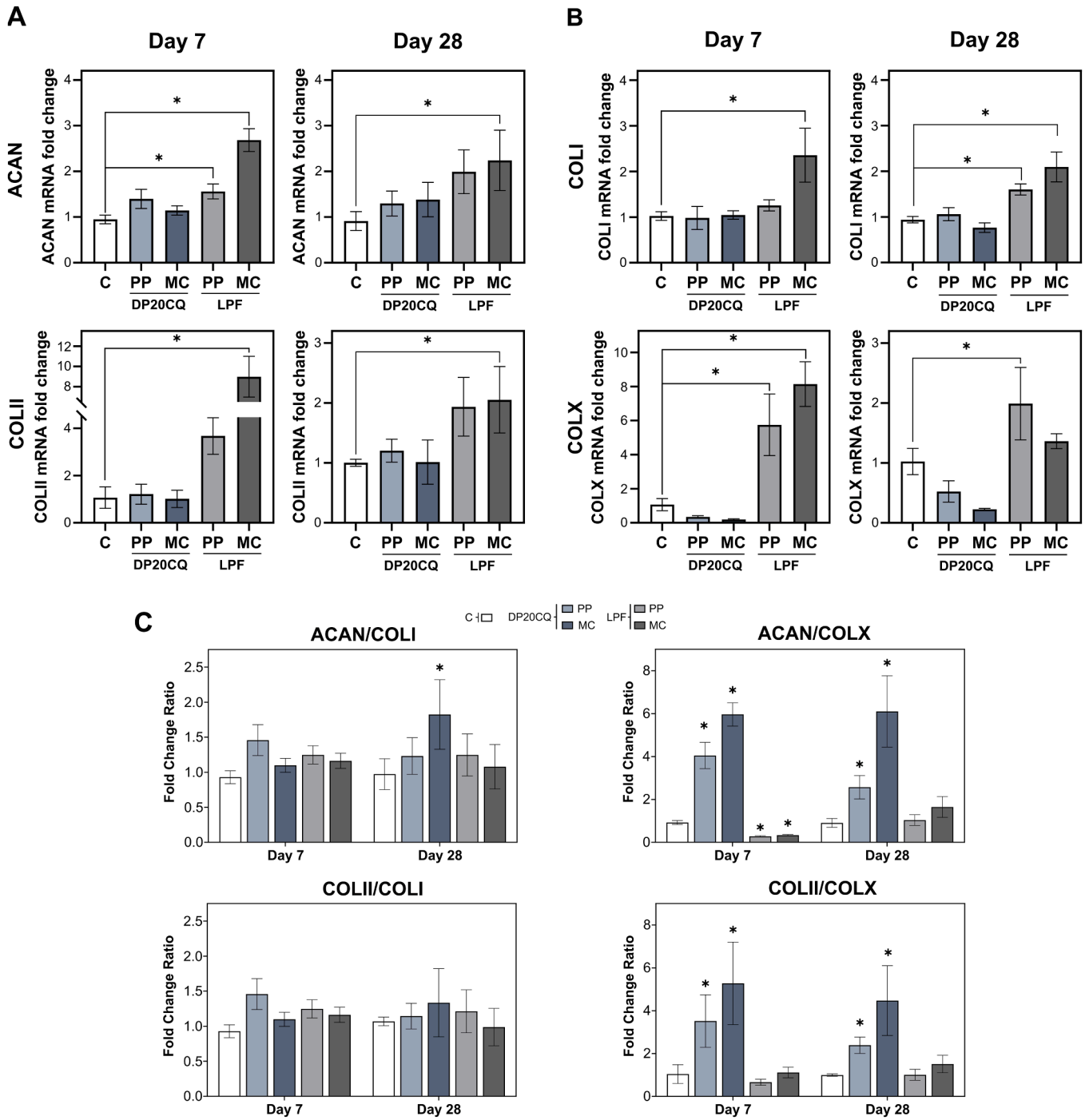

Fig. 6. qPCR analyses of chondrogenesis in CI/CII-HyA gene-activated scaffolds. RT-qPCR analysis of gene-activated scaffolds cultured 7 (left panels) and 28 (right panels) days in chondrogenic medium (negative control, C; white) and transfected with niosomes based on polysorbate 20 and chloroquine (DP20CQ; blue) or Lipofectamine (LPF; grey) and complexed with either parental plasmid (PP; light blue or light grey, respectively) or minicircle (MC; dark blue or dark grey, respectively) containing SOX9. Expression (bars) of (**A**) chondrogenic markers, such as aggrecan (ACAN) and type-II collagen (COLII), and (**B**) hypertrophy markers such as type-I (COLI) and type-X collagen (COLX). Ct values were normalized to GADPH, and fold inductions were calculated considering $2^{-\Delta\Delta Ct}$ method relative to the negative control. (**C**) Fold change (bars) of gene expression ratios: ACAN/COLI and ACAN/COLX (upper panels), COLII/COLI and COLII/COLX (lower panels). Data were normalised to gene-free scaffold on its corresponding day of culture. * depicts $p < 0.05$ when compared to the negative control (C), n = 3.

$p < 0.001$), indicating that cell viability was not affected under gene-activated conditions.

To better elucidate how treatment conditions affected cellular extracellular matrix (ECM) - proteoglycan deposition, proteoglycan levels were normalised to DNA content and expressed as fold change compared to the gene-free control (Fig. 7**B**). Proteoglycan/DNA ratio was increased in gene-activated scaffolds relative to the gene-free control (up to 1.16-fold change). PP-based scaffolds showed slightly higher values than MC counterparts, with DP20CQ/PP exhibiting the highest increase (1.23-fold), although these differences were not statistically significant.

Lastly, histological and immunohistochemical analyses after 28 days confirmed enhanced cartilage-like matrix formation in gene-activated scaffolds (Fig. 8). Alcian Blue staining intensity was significantly

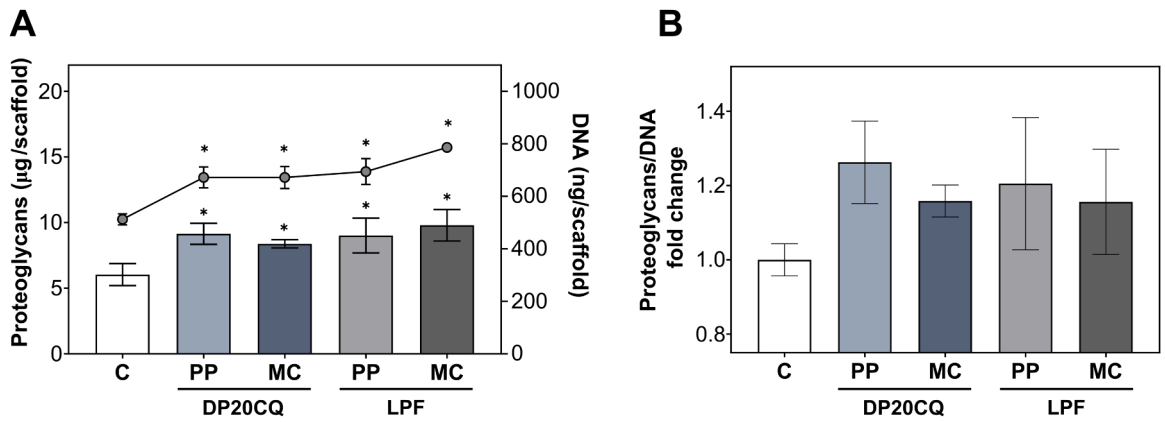

Fig. 7. Proteoglycan and DNA content in CI/CII-HyA gene-Activated Scaffolds. (**A**) Proteoglycan concentration (µg/scaffold; bars; left y-axis) and DNA content (ng/scaffold; symbols and lines; right y-axis) in gene-activated scaffolds cultured for 28 days in chondrogenic medium (negative control, C; white) and transfected with niosomes based on polysorbate 20 and chloroquine (DP20CQ; blue) or Lipofectamine (LPF; grey) and complexed with either parental plasmid (PP; light blue or light grey, respectively) or minicircle (MC; dark blue or dark grey, respectively). (**B**) Fold change (bars) of proteoglycan content normalized to DNA, relative to the negative control.* depicts $p < 0.05$ when compared to the negative control (C), n = 3.

increased in all transfected groups compared to controls ($p < 0.015$), although no significant differences were obtained between delivery systems (Fig. 8**A** and **C**).

Similarly, COLII immunostaining revealed significantly higher mean pixel intensity values in DP20CQ- and LPF-based scaffolds compared to gene-free controls ($p < 0.001$) (Fig. 8**A** and **C**). Moreover, within the same niosome-based formulation, PP-based scaffolds demonstrated marked immunoreactivity compared to MC-based scaffolds ($p < 0.04$).

In contrast, fibrocartilage and hypertrophy markers (Fig. 8**B** and **D**) were reduced in DP20CQ-based scaffolds. COLI immunoreactivity was significantly lower in DP20CQ scaffolds compared to both gene-free and LPF scaffolds ($p < 0.001$). Likewise, COLX staining was lowest in DP20CQ scaffolds ($p < 0.001$) and highest in LPF scaffolds ($p < 0.008$), further supporting a more stable chondrogenic phenotype in niosome-based systems.

4. Discussion

A major challenge in cartilage tissue engineering is the development of instructive biomaterials capable of promoting robust *de novo* matrix formation while preventing hypertrophic differentiation [3,27,39]. To address this, we integrated a collagen type I/II-hyaluronic acid (CI/CII-HyA) scaffold, with proven capacity to support effective chondrogenesis, with a non-viral gene delivery platform based on niosomes (DP20CQ) complexed with either parental (PP) or minicircle (MC) SOX9 plasmids to guide MSC-mediated chondrogenesis in a 3D environment. To the best of our knowledge, this is the first study to investigate the performance of niosomes to deliver different plasmid architectures, parental and minicircle plasmids, within a 3D biomimetic scaffold for cartilage repair.

Within the landscape of developing novel non-viral gene delivery systems, our group conducted an exhaustive screening of a niosome library to identify the most effective candidates for human MSC transfection. From this systematic evaluation, we successfully identified two DOTMA-based formulations, specifically those incorporating either polysorbate 20 or 80 as non-ionic surfactants alongside chloroquine or cholesterol as helper lipids (DP20CQ and DP80CH, respectively), as the most effective nanocarriers [18,19].

Given that transfection efficiency is significantly influenced by both the cell source and the specific plasmid architecture, in the present study, we first evaluated both formulations complexed with either parental (PP) or minicircle (MC) plasmids.

These initial assessments were conducted in MSC monolayers derived from early postnatal and juvenile donors to account for potential age-related biological variations.

DP20CQ formulation at a DOTMA/DNA ratio of 10/1 achieved the highest transfection efficiency, independent of donor age or plasmid architecture. This result aligns with our previous findings in human primary MSCs [19], where DP20CQ outperformed DP80CH despite comparable efficiencies in immortalised MSCs [18]. Consistent with earlier reports, P20 exhibits a higher hydrophilic-lipophilic balance (HLB), enhanced colloidal stability, and more efficient intracellular trafficking compared to P80 [40,41]. Such differences, together with the known endosomal-escape effects of chloroquine, may collectively contribute to the superior performance of DP20CQ across primary MSC populations in which endosomal escape is generally lower than in immortalised cells [42,43].

Together, results from MSC monolayer cultures, along with our previous observations demonstrating efficient SOX9 delivery by DP20CQ in aggregate cultures, identify DP20CQ formulation as the most reliable candidate for subsequent 3D studies [10,18,19].

Recent reports have shown that minicircles encoding chondrogenic factors (SOX9, BMP2, TGFβ3) can effectively drive chondrogenesis in a range of MSC-like cell types, including induced pluripotent stem cell-derived MSCs, as well as canine and equine MSCs [44,45]. While these findings underscore the versatility of minicircle-based gene delivery across species and cell sources, they remain largely confined to conventional 2D monolayers or 3D aggregate-based systems. In line with this, our previous studies demonstrated that SOX9 MC plasmids promoted comparable chondrogenic outcomes to those observed with PP in hMSC aggregate cultures [19].

Despite these promising results, the potential of MC vectors to promote *in situ* transfection within 3D biomimetic matrices remains largely unexplored. Unlike dense cell aggregates, biomimetic 3D scaffolds present a unique set of properties, including the physiological microenvironment, spatial constraints, and diffusion limitations, that may critically dictate the kinetics and overall efficiency of gene delivery. Beyond influencing gene transfer efficiency, these distinctive scaffold features position biomimetic 3D matrices as supportive microenvironments that facilitate cell infiltration, matrix remodelling, and localised gene delivery, thereby enabling gene-driven chondrogenic differentiation and contributing to cartilage reparative processes.

In order to be utilised effectively for gene delivery, to enable efficient *in situ* transfection, the scaffold must provide a 3D microenvironment that supports cell attachment and long-term viability while allowing efficient vector diffusion and cellular internalisation. SEM analysis revealed that the CI/CII-HyA scaffolds possessed a highly porous, interconnected architecture typical of collagen-based matrices produced

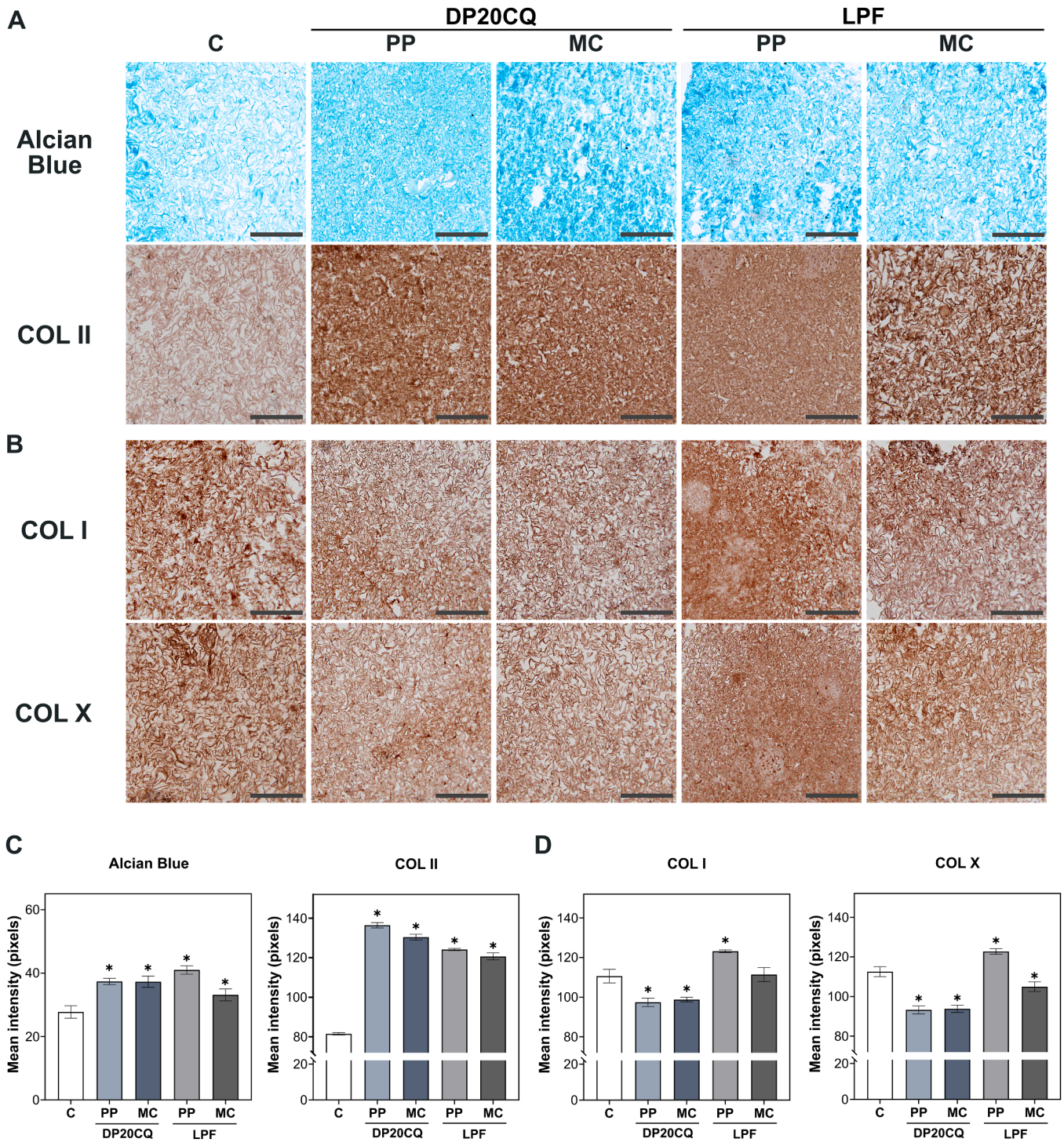

Fig. 8. Immunohistochemical and histological analyses of chondrogenesis in CI/CII-HyA gene-activated scaffolds. Immunohistochemical and histological analyses of gene-activated scaffolds after 28 days in chondrogenic medium (negative control, C; white) and transfected with niosomes based on polysorbate 20 and chloroquine (DP20CQ; blue) or Lipofectamine (LPF; grey) and complexed with either parental plasmid (PP; light blue or light grey, respectively) or minicircle (MC; dark blue or dark grey, respectively). (**A**) Alcian Blue and immunodetection of type-II collagen (COLII), (**B**) immunodetection of type-I collagen (COLI) and type-X collagen (COLX) (magnification 10x; scale bar: 200 μm). (**C** and **D**) Histomorphometric quantification (bars) corresponds to the images shown. Data are shown as mean ± SD. * depicts $p < 0.05$, when compared to the negative control (C), n = 3.

via lyophilisation [27]. Crucially, the incorporation of DP20CQ nioplexes did not alter this microarchitecture, preserving the interconnectivity essential for nutrient diffusion and waste removal. This observation aligns with previous studies demonstrating that non-viral vector loading via soak-loading or direct incorporation preserves the structural integrity of collagen-based scaffolds [25].

Retention of effective biocompatibility is a major concern when transitioning from 2D transfection to 3D gene-activated scaffolds. DP20CQ-activated scaffolds supported cell attachment efficiencies comparable to gene-free controls, indicating that the niosome coating did not mask the cell-binding motifs inherent to the scaffold.

Furthermore, metabolic activity assays demonstrated sustained

cellular viability and proliferation over the 28-day culture period. From 0.25–7 days, DP20CQ-activated scaffolds exhibited significantly higher metabolic activity than LPF-activated scaffolds ($p < 0.05$), indicating a reduced cytotoxic effect compared to liposomal formulations [10,46]. Beyond day 7, metabolic levels became comparable between the two groups, with no significant differences observed, indicating that the early differences were primarily driven by the initial toxicity profile of these nanocarriers.

The CI/CII-HyA scaffolds used in this study have previously been shown to guide an effective human MSC chondrogenesis with reduced hypertrophy and calcified cartilage-like formation after 28 days of culture [26]. In this framework, examining SOX9 expression and its downstream chondrogenic and hypertrophic markers at early (day 7) and late (day 28) time points provides a meaningful readout of the combined influence of the scaffold, delivery vector, and plasmid architecture, and enables the assessment of whether the delivery of the gene therapeutics can further enhance the regenerative capacity of the scaffold.

qRT-PCR analysis demonstrated that DP20CQ-based scaffolds enabled remarkably efficient transfection in a 3D microenvironment, achieving superior SOX9 expression levels at days 7 and 28 compared to gene-free scaffolds and LPF-activated scaffolds. These transcriptional trends align with the behaviour of DP20CQ-activated scaffolds, which is characterised by a pronounced initial burst followed by sustained plasmid release [10,47], in contrast to the more modest burst observed in LPF-loaded scaffolds. This release profile may be associated with the higher and more sustained overexpression of the chondrogenic factor observed in niosome-based scaffolds. Moreover, this pattern is particularly relevant for chondrogenesis, as an early and robust SOX9 expression is required to initiate lineage commitment, while prolonged expression supports extracellular matrix deposition and phenotypic stabilisation. Western blot analysis supported this observation, showing that bands corresponding to DP20CQ-activated scaffolds had higher intensity than those of LPF-activated scaffolds.

When comparing both plasmid architectures, DP20CQ-activated scaffolds exhibited a faster release of PP than MC DNA. This difference is likely related to differences in nioplexe stability associated with plasmid size and topology. In our previous work [19], DP20CQ nioplexes formed with MC displayed a smaller hydrodynamic diameter than those with PP at a DOTMA/DNA ratio of 10/1, indicating the formation of more compact complexes. Moreover, DNase I protection assays revealed that MC nioplexes remained partially retained in the loading wells even after SDS treatment, suggesting a higher resistance to complex dissociation [19]. Together, these findings support that the supercoiled structure of MC promotes the formation of more stable nioplexes, resulting in a slower release profile compared with PP.

In situ SOX9 overexpression via DP20CQ-activated scaffolds induced a robust chondrogenic response, evidenced by the marked upregulation of its downstream targets ACAN and COLII, and by enhanced proteoglycan deposition at day 28. Alongside, DP20CQ-activated scaffolds led to a marked reduction of fibrocartilage (COLI) and hypertrophy (COLX) markers, at both gene and protein levels. As a result, chondrogenic-to-hypertrophic ratios provided an integrated assessment of marker regulation, confirming that niosome-activated scaffolds, particularly those incorporating MC plasmids, promoted a more stable hyaline-like cartilage phenotype than LPF-based systems. These differences likely reflect distinct vector architectures and delivery kinetics, with DP20CQ-based niosomes appearing more compatible with the diffusion-limited and matrix-rich environment of 3D scaffolds [10,11].

These observations are consistent with previous studies in hMSC aggregate cultures and niosome-activated cryogels [10,11,19], where sustained SOX9 expression was directly associated with enhanced hyaline cartilage formation and suppression of hypertrophic progression. Importantly, the present system achieves similar trends in chondrogenic differentiation, characterised by the upregulation of cartilage-specific markers and suppression of hypertrophic markers, using the delivery of a single SOX9 plasmid, whereas earlier strategies required either the simultaneous delivery of the SOX Trio (SOX5/6/9) [9] or the use of poly-ε-caprolactone mechanically reinforced CI/CII-HyA scaffolds [25].

From a translational perspective, these findings support that DP20CQ-activated CI/CII–HyA scaffolds may enable localised SOX9 delivery to bone marrow–derived MSCs infiltrating the scaffold, promoting site-specific chondrogenic differentiation. Beyond its utility in SOX9-mediated cartilage repair, the versatility of the DP20CQ non-viral vector highlights its potential for delivering alternative minicircle-encoded therapeutic genes in combination with diverse biomaterial platforms, broadening its applicability in tissue engineering strategies. In this context, the integration of localised gene delivery within an instructive scaffold framework represents an effective means of further enhancing the intrinsic regenerative capacity of biomaterial-based repair approaches.

Although *in vivo* validation is still required to confirm long-term functional cartilage repair and integration, the present results provide a robust *in vitro* proof-of-concept supporting the further development of this non-viral gene-activated scaffold platform.

5. Conclusion

Taken together, the present study demonstrates that DP20CQ-activated CI/CII-HyA scaffolds constitute an effective non-viral platform for localised gene delivery and MSC-mediated chondrogenesis within a biomimetic 3D environment. DP20CQ-based systems promoted sustained SOX9 expression and enhanced chondrogenic differentiation, characterised by increased hyaline-like cartilage-associated markers expression and reduced fibrocartilaginous and hypertrophic progression compared to LPF-based formulations. Notably, minicircle-based systems displayed improved chondrogenic-to-hypertrophic ratios, supporting the relevance of plasmid architecture in diffusion-limited 3D environments. Overall, the combination of a biomimetic collagen-based scaffold with a stable niosome-mediated delivery platform highlights the potential of this strategy for the development of next-generation gene-activated scaffolds for cartilage repair. Although *in vivo* validation remains necessary, the present findings provide a robust in vitro proof-of-concept supporting further translational development.

CRediT authorship contribution statement

Junquera López-Seijas: Writing – review & editing, Writing – original draft, Methodology, Investigation, Data curation. **Alba Iglesias-Fente:** Writing – review & editing, Writing – original draft, Data curation. **Ana Rey-Rico:** Writing – review & editing, Writing – original draft, Supervision, Project administration, Formal analysis, Conceptualization. **Marko Dobricic:** Writing – review & editing, Methodology. **Fergal O'Brien:** Writing – review & editing, Conceptualization. **Claudio Intini:** Writing – review & editing, Methodology.

Funding sources

This work was supported by MCIN/AEI/10.13039/501100011033 [RYC2018–025617-I] and MCIN/AEI/10.13039/501100011033 [CNS2024–154660]. Junquera López-Seijas acknowledges MCIN [FPU20/06176], and Alba Iglesias-Fente thanks Xunta de Galicia (ED481A 2022/041) for their Pre-doctoral Fellowship Grants.

Declaration of Competing Interest

The authors declare the following financial interests/personal relationships which may be considered as potential competing interests: Ana Rey Rico reports article publishing charges was provided by University of A Coruña. If there are other authors, they declare that they have no known competing financial interests or personal relationships that could have appeared to influence the work reported in this paper.

Acknowledgements

We thank Dr. Juan Fafián Labora and Dra. María Arufe for their support in rat MSCs isolation and Universidade da Coruña/CISUG for the funding for open access charge.

Appendix A. Supporting information

Supplementary data associated with this article can be found in the online version at doi:10.1016/j.colsurfb.2026.115909.

Data Availability

Data will be made available on request.

References

[1] H. Le, W. Xu, X. Zhuang, F. Chang, Y. Wang, J. Ding, Mesenchymal stem cells for cartilage regeneration, J. Tissue Eng. 11 (2020) 2041731420943839, https://doi.org/10.1177/2041731420943839.
[2] Z. Su, T. Yang, X. Wu, P. Liu, Y. Nuermaimaiti, Y. Ran, P. Wang, P. Cao, Comparative Analysis and Regeneration Strategies for Three Types of Cartilage, Tissue Eng. Part. B Rev. 31 (2025) 221–233, https://doi.org/10.1089/ten.TEB.2024.0140.
[3] M. Wang, J. Wang, X. Xu, E. Li, P. Xu, Engineering gene-activated bioprinted scaffolds for enhancing articular cartilage repair, Mater. Today Bio 29 (2024) 101351, https://doi.org/10.1016/j.mtbio.2024.101351.
[4] M. Janitermi, S.G.A. Jorsarai, E. Fattahi, Chondrogenic Differentiation of Mesenchymal Stem Cells from Rat Bone Marrow on the Elastic Modulus of Electrospun Silk Fibroin Scaffolds, Regen. Eng. Transl. Med. 8 (2022) 125–133, https://doi.org/10.1007/s40883-021-00199-x.
[5] A. Rey-Rico, J.K. Venkatesan, J. Frisch, I. Rial-Hermida, G. Schmitt, A. Concheiro, H. Madry, C. Alvarez-Lorenzo, M. Cucchiarini, PEO–PPO–PEO micelles as effective rAAV-mediated gene delivery systems to target human mesenchymal stem cells without altering their differentiation potency, Acta Biomater. 27 (2015) 42–52, https://doi.org/10.1016/J.ACTBIO.2015.08.046.
[6] D.C. Kelly, R.M. Raftery, C.M. Curtin, C.M. O'Driscoll, F.J. O'Brien, Scaffold-Based Delivery of Nucleic Acid Therapeutics for Enhanced Bone and Cartilage Repair, J. Orthop. Res. 37 (2019) 1671–1680, https://doi.org/10.1002/jor.24321.
[7] M. Cucchiarini, H. Madry, Biomaterial-guided delivery of gene vectors for targeted articular cartilage repair, Nat. Rev. Rheumatol. 15 (2019) 18–29, https://doi.org/10.1038/s41584-018-0125-2.
[8] H. Madry, J.K. Venkatesan, N. Carballo-Pedrares, A. Rey-Rico, M. Cucchiarini, Scaffold-Mediated Gene Delivery for Osteochondral Repair, Pharmaceutics 12 (2020) 930, https://doi.org/10.3390/pharmaceutics12100930.
[9] R.M. Raftery, A.G. Gonzalez Vazquez, G. Chen, F.J. O'Brien, Activation of the SOX-5, SOX-6, and SOX-9 Trio of Transcription Factors Using a Gene-Activated Scaffold Stimulates Mesenchymal Stromal Cell Chondrogenesis and Inhibits Endochondral Ossification, Adv. Healthc. Mater. 9 (2020) e1901827, https://doi.org/10.1002/adhm.201901827.
[10] N. Carballo-Pedrares, J. López-Seijas, D. Miranda-Balbuena, I. Lamas, J. Yáñez, A. Rey-Rico, Gene-activated hyaluronic acid-based cryogels for cartilage tissue engineering, J. Control. Release 362 (2023) 606–619, https://doi.org/10.1016/J.JCONREL.2023.09.008.
[11] N. Carballo-Pedrares, C. Sanjurjo-Rodriguez, J. Señarís, S. Díaz-Prado, A. Rey-Rico, Chondrogenic Differentiation of Human Mesenchymal Stem Cells via SOX9 Delivery in Cationic Niosomes, Pharmaceutics 14 (2022) 2327, https://doi.org/10.3390/PHARMACEUTICS14112327/S1.
[12] A. Haseeb, R. Kc, M. Angelozzi, C. de Charleroy, D. Rux, R.J. Tower, L. Yao, R. Pellegrino da Silva, M. Pacifici, L. Qin, V. Lefebvre, SOX9 keeps growth plates and articular cartilage healthy by inhibiting chondrocyte dedifferentiation/osteoblastic redifferentiation, Proc. Natl. Acad. Sci. 118 (2021) e2019152118, https://doi.org/10.1073/pnas.2019152118.
[13] W. Zhang, Y. Hou, S. Yin, Q. Miao, K. Lee, X. Zhou, Y. Wang, Advanced gene nanocarriers/scaffolds in nonviral-mediated delivery system for tissue regeneration and repair, J. Nanobiotechnol 22 (2024) 376, https://doi.org/10.1186/s12951-024-02580-8.
[14] Y. Jin, W. Yu, W. Zhang, C. Wang, Y. Liu, W.-E. Yuan, Y. Feng, A novel fluorinated polyethyleneimine with microRNA-942-5p-sponges polyplex gene delivery system for non-small-cell lung cancer therapy, J. Colloid Interface Sci. 648 (2023) 287–298, https://doi.org/10.1016/j.jcis.2023.05.153.
[15] S. Shtykalova, D. Deviatkin, S. Freund, A. Egorova, A. Kiselev, Non-Viral Carriers for Nucleic Acids Delivery: Fundamentals and Current Applications, Life (Basel Switz.) 13 (2023), https://doi.org/10.3390/LIFE13040903.
[16] W. Zhang, Y. Jin, J. Wang, M. Gu, Y. Wang, X. Zhang, Y. Zhang, W. Yu, Y. Liu, W.-E. Yuan, J. Su, Co-delivery of PROTAC and siRNA via novel liposomes for the treatment of malignant tumors, J. Colloid Interface Sci. 678 (2025) 896–907, https://doi.org/10.1016/j.jcis.2024.08.185.
[17] S. Grijalvo, G. Puras, J. Zárate, M. Sainz-Ramos, N.A.L. Qtaish, T. López, M. Mashal, N. Attia, D. Díaz, R. Pons, E. Fernández, J.L. Pedraz, R. Eritja, Cationic Niosomes as Non-Viral Vehicles for Nucleic Acids: Challenges and Opportunities in Gene Delivery, Pharmaceutics 11 (2019) 50, https://doi.org/10.3390/pharmaceutics11020050.
[18] J. López-Seijas, A. Iglesias-Fente, D. Miranda-Balbuena, A. Rey-Rico, Exploiting niosomes as efficient non-viral vectors for enhanced gene transfer to human mesenchymal stem cells, J. Drug. Deliv. Sci. Technol. 107 (2025) 106766, https://doi.org/10.1016/j.jddst.2025.106766.
[19] J. López-Seijas, A. Iglesias-Fente, A. Ramil-Bouzas, S. Paniagua-Barro, J. Fafián-Labora, A. Rey-Rico, Targeted chondrogenic differentiation of human MSCs using niosomes for SOX9 gene delivery: comparison of minicircle and conventional plasmids, Stem Cell. Res. Ther. (2025), https://doi.org/10.1186/s13287-025-04867-5.
[20] C.L. Hardee, L.M. Arévalo-Soliz, B.D. Hornstein, L. Zechiedrich, Advances in Non-Viral DNA Vectors for Gene Therapy, Genes. (Basel) 8 (2017) 65, https://doi.org/10.3390/genes8020065.
[21] X. Guan, Y. Pei, J. Song, DNA-Based Nonviral Gene Therapy—Challenging but Promising, Mol. Pharm. 21 (2024) 427–453, https://doi.org/10.1021/acs.molpharmaceut.3c00907.
[22] M. Florian, J.-P. Wang, Y. Deng, L. Souza-Moreira, D.J. Stewart, S.H.J. Mei, Gene engineered mesenchymal stem cells: greater transgene expression and efficacy with minicircle vs. plasmid DNA vectors in a mouse model of acute lung injury, Stem Cell. Res. & Ther. 12 (2021) 184, https://doi.org/10.1186/s13287-021-02245-5.
[23] P. Chanani, N. Rezaei, K. Dormiani, M. Shokatian, N.S. Ata-abadi, Progress and prospect of minicircle as a minimized non-viral DNA vector in gene therapy and regenerative medicine, Mol. Ther. Nucleic Acids 36 (2025), https://doi.org/10.1016/j.omtn.2025.102682.
[24] R.M. Raftery, D.P. Walsh, L. Blokpoel Ferreras, I. Mencía Castaño, G. Chen, M. LeMoine, G. Osman, K.M. Shakesheff, J.E. Dixon, F.J. O'Brien, Highly versatile cell-penetrating peptide loaded scaffold for efficient and localised gene delivery to multiple cell types: From development to application in tissue engineering, Biomaterials 216 (2019) 119277, https://doi.org/10.1016/J.BIOMATERIALS.2019.119277.
[25] M. Joyce, T. Hodgkinson, C. Intini, J. Dixon, D. Kelly, F. O'Brien, Gene activated reinforced scaffolds for SOX9 delivery to enhance repair of large load bearing articular cartilage defects, Eur. Cell. Mater. 47 (2024) 91–108, https://doi.org/10.22203/eCM.v047a07.
[26] C. Intini, T. Hodgkinson, S.M. Casey, J.P. Gleeson, F.J. O'brien, Highly Porous Type II Collagen-Containing Scaffolds for Enhanced Cartilage Repair with Reduced Hypertrophic Cartilage Formation, Bioengineering 9 (2022) 232, https://doi.org/10.3390/BIOENGINEERING9060232, 2022, Vol. 9, Page 232.
[27] C. Intini, M. Lemoine, T. Hodgkinson, S. Casey, J.P. Gleeson, F.J. O'Brien, A highly porous type II collagen containing scaffold for the treatment of cartilage defects enhances MSC chondrogenesis and early cartilaginous matrix deposition, Biomater. Sci. 10 (2022) 970–983, https://doi.org/10.1039/D1BM01417J.
[28] C. Intini, M. Joyce, M. Uberti, M.C. Labberté, G. Brunetti, B. Hackett, T. Hodgkinson, J.M. O'Byrne, P.A.J. Brama, F.J. O'Brien, A biomimetic reinforced type I/II collagen and hyaluronic acid scaffold in combination with a chondral biomaterial fixation technique for large articular cartilage defect repair: A pilot pre-clinical study, Int. J. Biol. Macromol. 318 (2025) 145302, https://doi.org/10.1016/j.ijbiomac.2025.145302.
[29] C. Lian, X. Wang, X. Qiu, Z. Wu, B. Gao, L. Liu, G. Liang, H. Zhou, X. Yang, Y. Peng, A. Liang, C. Xu, D. Huang, P. Su, Collagen type II suppresses articular chondrocyte hypertrophy and osteoarthritis progression by promoting integrin β1−SMAD1 interaction, Bone Res. 7 (2019) 8, https://doi.org/10.1038/s41413-019-0046-y.
[30] M.A. Kay, C.-Y. He, Z.-Y. Chen, A robust system for production of minicircle DNA vectors, Nat. Biotechnol. 28 (2010) 1287–1289, https://doi.org/10.1038/nbt.1708.
[31] V.M. Gaspar, C.J. Maia, J.A. Queiroz, C. Pichon, I.J. Correia, F. Sousa, Improved minicircle DNA biosynthesis for gene therapy applications, Human. Gene Ther. Methods 25 (2014) 93–105, https://doi.org/10.1089/HGTB.2013.020.
[32] H. Mitdank, S. Sama, M. Tröger, M.F. Testa, M. Ferrarese, D. Balestra, M. Pinotti, A. Weng, An advanced method for the small-scale production of high-quality minicircle DNA, Int. J. Pharm. 605 (2021) 120830, https://doi.org/10.1016/j.ijpharm.2021.120830.
[33] Y. Thabet, M. Elsabahy, N.G. Eissa, Methods for preparation of niosomes: A focus on thin-film hydration method, Methods 199 (2022) 9–15, https://doi.org/10.1016/J.YMETH.2021.05.004.
[34] A. Matsiko, T.J. Levingstone, F.J. O'Brien, J.P. Gleeson, Addition of hyaluronic acid improves cellular infiltration and promotes early-stage chondrogenesis in a collagen-based scaffold for cartilage tissue engineering, J. Mech. Behav. Biomed. Mater. 11 (2012) 41–52, https://doi.org/10.1016/J.JMBBM.2011.11.012.
[35] Y.-Y. Liu, C. Intini, M. Dobricic, F.J. O'Brien, J. LLorca, M. Echeverry-Rendon, Collagen-based 3D printed poly (glycerol sebacate) composite scaffold with biomimicking mechanical properties for enhanced cartilage defect repair, Int. J. Biol. Macromol. 280 (2024) 135827, https://doi.org/10.1016/j.ijbiomac.2024.135827.
[36] D. Miranda-Balbuena, A. Ramil-Bouzas, N. Doldán-Mata, J. López-Seijas, J. Fafián-Labora, I. Lamas-Criado, J.-R. Caeiro-Rey, P. Fernández-Trillo, A. Rey-Rico, Novel PEI-aldehyde conjugates for gene delivery: Promoting chondrogenic differentiation in human mesenchymal stem cells, Mol. Ther. Nucleic Acids 36 (2025), https://doi.org/10.1016/j.omtn.2025.102551.
[37] C. Intini, L.B. Ferreras, S. Casey, J.E. Dixon, J.P. Gleeson, F.J. O'Brien, An Innovative miR-Activated Scaffold for the Delivery of a miR-221 Inhibitor to Enhance Cartilage Defect Repair, Adv. Ther. 6 (2023) 2200329, https://doi.org/10.1002/adtp.202200329.
[38] S. An, C. Intini, D. O'Shea, J.E. Dixon, Y. Zheng, F.J. O'Brien, A miR-activated hydrogel for the delivery of a pro-chondrogenic microRNA-221 inhibitor as a

minimally invasive therapeutic approach for articular cartilage repair, Mater. Today Bio 30 (2025) 101382, https://doi.org/10.1016/j.mtbio.2024.101382.
[39] M. Wang, Y. Wu, G. Li, Q. Lin, W. Zhang, H. Liu, J. Su, Articular cartilage repair biomaterials: strategies and applications, Mater. Today Bio 24 (2024) 100948, https://doi.org/10.1016/j.mtbio.2024.100948.
[40] I. Villate-Beitia, I. Gallego, G. Martínez-Navarrete, J. Zárate, T. López-Méndez, C. Soto-Sánchez, E. Santos-Vizcaíno, G. Puras, E. Fernández, J.L. Pedraz, Polysorbate 20 non-ionic surfactant enhances retinal gene delivery efficiency of cationic niosomes after intravitreal and subretinal administration, Int. J. Pharm. 550 (2018) 388–397, https://doi.org/10.1016/j.ijpharm.2018.07.035.
[41] O. Paecharoenchai, N. Niyomtham, L. Leksantikul, T. Ngawhirunpat, T. Rojanarata, B. Yingyongnarongkul, P. Opanasopit, Nonionic surfactant vesicles composed of novel spermine-derivative cationic lipids as an effective gene carrier in vitro, AAPS PharmSciTech 15 (2014) 722–730, https://doi.org/10.1208/s12249-014-0095-x.
[42] M. Mashal, N. Attia, G. Martínez-Navarrete, C. Soto-Sánchez, E. Fernández, S. Grijalvo, R. Eritja, G. Puras, J.L. Pedraz, Gene delivery to the rat retina by non-viral vectors based on chloroquine-containing cationic niosomes, J. Control. Release Off. J. Control. Release Soc. 304 (2019) 181–190, https://doi.org/10.1016/J.JCONREL.2019.05.010.
[43] X. Yang, X. Wen, J. Dai, Y. Chen, W. Ding, J. Wang, X. Gu, X. Zhang, J. Chen, R. L. Sutliff, S.R. Emory, G. Ruan, Probing the Intracellular Delivery of Nanoparticles into Hard-to-Transfect Cells, ACS Nano 16 (2022) 8751–8765, https://doi.org/10.1021/acsnano.1c07648.
[44] N. Tidd, J. Michelsen, B. Hilbert, J.C. Quinn, Minicircle Mediated Gene Delivery to Canine and Equine Mesenchymal Stem Cells, Int. J. Mol. Sci. 18 (2017) 819, https://doi.org/10.3390/IJMS18040819.
[45] Y.A. Rim, Y. Nam, N. Park, H. Jung, K. Lee, J. Lee, J.H. Ju, Chondrogenic Differentiation from Induced Pluripotent Stem Cells Using Non-Viral Minicircle Vectors, Cells 9 (2020) 582, https://doi.org/10.3390/CELLS9030582.
[46] S. Chameettachal, S. Midha, S. Ghosh, Regulation of Chondrogenesis and Hypertrophy in Silk Fibroin-Gelatin-Based 3D Bioprinted Constructs, ACS Biomater. Sci. Eng. 2 (2016) 1450–1463, https://doi.org/10.1021/acsbiomaterials.6b00152.
[47] E.J. Sheehy, G.J. Miller, I. Amado, R.M. Raftery, G. Chen, K. Cortright, A. G. Vazquez, F.J. O'Brien, Mechanobiology-informed regenerative medicine: Dose-controlled release of placental growth factor from a functionalized collagen-based scaffold promotes angiogenesis and accelerates bone defect healing, J. Control. Release 334 (2021) 96–105, https://doi.org/10.1016/j.jconrel.2021.03.031.